PREDICTING PROCESS-INDUCED DEFORMATIONS WITH A COUPLED CURE-COMPACTION MODEL IN AFP-MANUFACTURED LAMINATES

Raúl A. Gómez-Quiñones[1*], Ekaterina Gongadze[1], Attilio Chiappini[2], Stephen R. Hallett[1] and Jonathan P.-H. Belnoue[1,3]

[1] Bristol Composites Institute, University of Bristol, Bristol, UK, [2] Airbus Atlantic, Colomiers, France, [3] National Composites Centre, Bristol, UK

* *Corresponding author (raulandres.gomezquinones@bristol.ac.uk)*

Keywords: *Process simulation, Toughened Prepreg, Consolidation, Spring-in, AFP*

1. Abstract

Automated Fiber Placement (AFP) processes are widely used to manufacture large composite structures which can comprise hundreds of layers of prepreg plies. A fully coupled cure and compaction model is developed to address challenges surrounding modelling the consolidation of toughened prepreg, building upon the DefGen ProToCoL model, and combined with a linear-elastic model to predict residual stresses. The model whilst initially phenomenological, now incorporates a physics-based reformulation to better capture material consolidation parameters. This study focuses on predicting the process induced deformations in L-brackets, namely the degree of spring-in after autoclave consolidation.

Implemented in Abaqus/Standard, the model is validated with previous experimental work used in the validation of the previous uncoupled iteration of the model. The autoclave consolidation of an L-bracket laminate was also simulated and compared with data from literature utilizing the same material system. Results show retained prediction accuracy and improved applicability, offering potential for streamlining design and manufacturing processes in the aerospace industry.

2. Introduction

Materials and automation technologies have outpaced understanding necessary to reliably predict and optimize manufacturing processes, which continue to rely on costly trial-and-error approaches. Automated Fibre Placement (AFP) is one such technology, consisting of a robot with a placement head that typically deposits prepreg tows. It is capable of manufacturing large composite structures at rates not feasible with traditional hand-layup methods, however, AFP part quality is sensitive to process conditions and tow trajectories. In thick laminates, layers of prepreg at the bottom of the laminate are also subject to more compaction from the AFP head's compaction roller passing over repeatedly as it deposits new layers of prepreg above, resulting in an initial non-uniform ply thickness distribution.

Modern multi-component composite systems such as thermoplastic-toughened thermoset prepregs have been introduced for improved mechanical performance. These types of material systems undergo large viscosity changes under typical AFP process conditions; they exhibit flow behaviours of thermosets and thermoplastics, able to percolate through fibres like thermosets at low viscosities (bleeding flow) and pushing fibres along as a highly viscous incompressible fluid like thermoplastics at higher viscosities (squeezing flow).

The high inter-dependence between various parameters as well as history dependence makes it difficult to simulate the cure & consolidation in one step, requiring multiple sequential analyses to accurately model. Furthermore, splitting the analysis into multiple, un-coupled steps may result in inaccuracies as the inter-dependence of material properties is not fully captured (e.g., fibre volume fraction will affect the overall conductivity of the material, which affects rate of cure, which then affects how the material compacts, and thus in turn the fibre volume fraction itself).

2.1. Reformulation of existing DefGen ProToCoL model

As final part geometry and quality of autoclave-cured composites are highly dependent on consolidation prior to resin gelation, a phenomenological model for predicting the compaction of thermoset-toughened prepregs, the DefGen ProToCoL model, was developed by Belnoue et. al. [1]. It is a hyper-viscoelastic material model that can capture the transition between bleeding and squeezing flow of uncured thermoset-toughened prepregs at a variety of processing conditions typical for AFP deposition. By taking geometrical considerations at both micro- and mesoscales, the model can describe both flow modes using expressions relating pressure with strain and strain-rate terms by assuming transition occurs upon the fibres reaching a critical point, becoming so tightly packed (fibre locking) that the material cannot compact any further. However, since the model was limited to temperatures where negligible resin cure occurs and relied on linearly interpolating material parameters for temperatures not covered during material characterization, it was not as suited for the simulation of a typical autoclave cure cycle.

Previously dependent on experimentally derived material parameters, a new physics-based reformulation was then derived by Belnoue et. al. [2] through a deeper analysis of the evolution of these parameters for a variety of different prepreg systems (ranging between thermoplastic, thermoset, and toughened thermosets). After reformulation, only three material parameters at a given temperature are required:

k - defined as the effective square size of fibres normalized to the size of the unit cell (microscale), now a function of resin viscosity:

$$k = \sqrt{V_f^0}\left(1 - \tanh\left(\frac{\eta_{\text{resin}}}{\eta_{\text{ph trans.}}} + 0.25\right)\right) + \sqrt{V_{f,\text{mp}}}\tanh\left(\frac{\eta_{\text{resin}}}{\eta_{\text{ph trans.}}} + 0.25\right) \quad (1)$$

a - a power law index that determines whether the material is pseudoplastic, Newtonian, or dilatant, now a function of temperature:

$$a = \frac{m_a}{RT} \tag{22}$$

$\bar{b}$ - a flow consistency index, related to an energy barrier that controls the transition between flow modes. Now a function of resin viscosity and temperature, it increases as the material becomes more viscous:

$$\bar{b} = \frac{\varepsilon_0^2}{1-\varepsilon_0} r_{apparent} \left[-16{,}628 \frac{T_{ph\ trans.}}{T} + 12{,}471\right] + \ln(\eta_{\text{resin}}) \tag{3}$$

One area of focus for this work was the integration of this new reformulated model into a usable simulation tool for a particular toughened aerospace prepreg system (Hexcel IMA/M21) subject to typical autoclave process conditions.

3. Coupling of Cure and Compaction

3.1. Resin Cure

A modified Kamal-Sourour autocatalytic cure kinetics model for M21 resin proposed by Mesogitis et. al. [3] was used for the estimation of degree of cure (Eq. 4). This cure kinetics model adds a diffusion term to better approximate diffusion rate-limitation effects at higher degrees of cure:

$$\frac{d\alpha}{dt} = k_1(1-\alpha)^{n_1} + k_2\alpha^m(1-\alpha)^{n_2}, \tag{4}$$

$$k_i = \left(\frac{1}{\frac{1}{k_{ic}} + \frac{1}{k_D}}\right), k_{iC} = A_i\, exp\left(-\frac{E_i}{RT}\right), \text{for } i = 1,2,D \tag{5}$$

3.2. Relevant Thermophysical Properties

Similarly, the resin and fibres' specific heat capacities (c_p) were estimated using expressions also proposed in [3] (Eqs. 5, 6). The specific heat capacity of the laminate was then calculated using a rule of mixtures (Eq. 7).

$$c_{p,r} = A_{r,c_p}T + B_{r,c_p} + \frac{\Delta_{r,c_p}}{1 + e^{C_{r,c_p}(T - T_g - s)}} \tag{6}$$

$$c_{p,f} = A_{f,c_p}T + B_{f,c_p} \tag{7}$$

$$c_p = w_f c_{p,f} + (1 - w_f)c_{p,r} \tag{8}$$

The thermal conductivity (λ) of IMA fibres was assumed to be like that of T300 fibres, and a simple linear model was used [4] (Eq. 8). M21 resin conductivity was estimated using an expression by Struzziero et. al. [5] (Eq. 9). Thermal conductivity in the fibre direction was calculated using a rule of mixtures (Eq. 10), and transverse and through-thickness conductivities were assumed to be equal using another relation by Mesogitis et. al. [3] (Eq. 11).

$$\lambda_f = A_{k_f}T + B_{k_f} \tag{9}$$

$$\lambda_r = A_{k_r}T\alpha + B_{k_r}T + c_{k_r}\alpha + D_{k_r} \tag{10}$$

$$\lambda_{11} = w_f\lambda_f + (1 - w_f)\lambda_r \tag{11}$$

$$\lambda_{22} = \lambda_{33} = A_kT + B_k\alpha + C_kT + D_k \tag{12}$$

3.3. Evolution of Viscosity

Following the computation of degree of cure, resin viscosity (η_{resin}) was estimated using a modified Castro-Macosko model [6] (Eq. 12):

$$\eta_{\text{resin}}(\alpha, T) = \varepsilon_{\eta,1}e^{\frac{E_{\eta,1}}{RT}} + \varepsilon_{\eta,2}e^{\frac{E_{\eta,2}}{RT}}\left(\frac{\alpha_{gel}}{\alpha_{gel} - \alpha}\right)^{A+B\alpha+C\alpha^2} \tag{13}$$

The model's parameters were determined using dynamic temperature viscosity measurements provided within the M21 datasheet by the prepreg manufacturer [7]. Experimentally derived viscosity data and the viscosity model's predictions are both shown in *Figure 1*. Values of the derived parameters are shown below in *Table 1*.

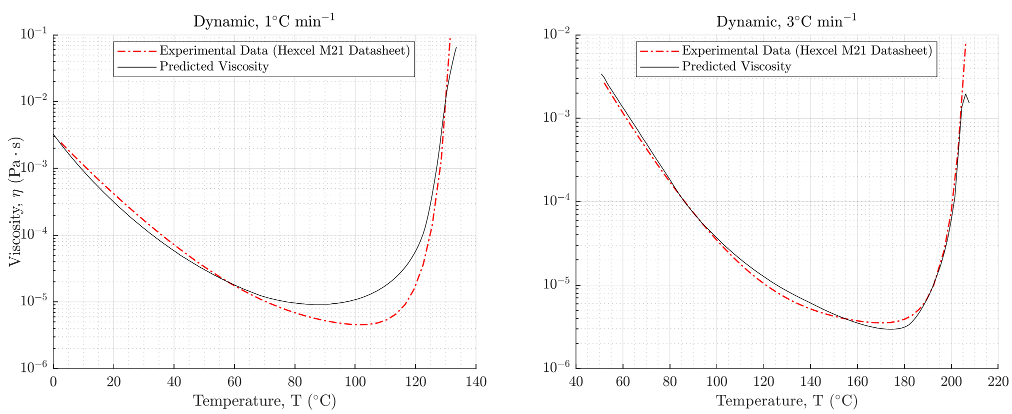

Figure 1. Measured [7] and predicted resin viscosity for 1°C min^{-1} and 3°C min^{-1} ramps.

Table 1. Resin viscosity model parameters.

Parameter (Units)	$\varepsilon_{\eta,1}$ (Pa s)	$E_{\eta,1}$ (J mol-1)	$\varepsilon_{\eta,2}$ (Pa s)	$E_{\eta,2}$ (J mol-1)	A (-)	B (-)	C (-)
Value	1.7954e^{-6}	94,450	1.1795e^{-3}	27,875	1.07	6.32e^{-4}	13.88

3.4. Material Parameter Estimation

With an adequate estimation of resin viscosity from temperature and resin cure, the predicted values for the model's material parameters could be compared to their experimentally measured values at varying temperatures, both within and outside the temperature range considered by Belnoue et. al. [1]. The variation of k, a, and $\bar{b}$ with temperature was calculated in a MATLAB script for a 1°C min^{-1} temperature ramp from 25-150°C, and is plotted below in *Fig. 2*, along with their respective experimental values measured between 30-90°C.

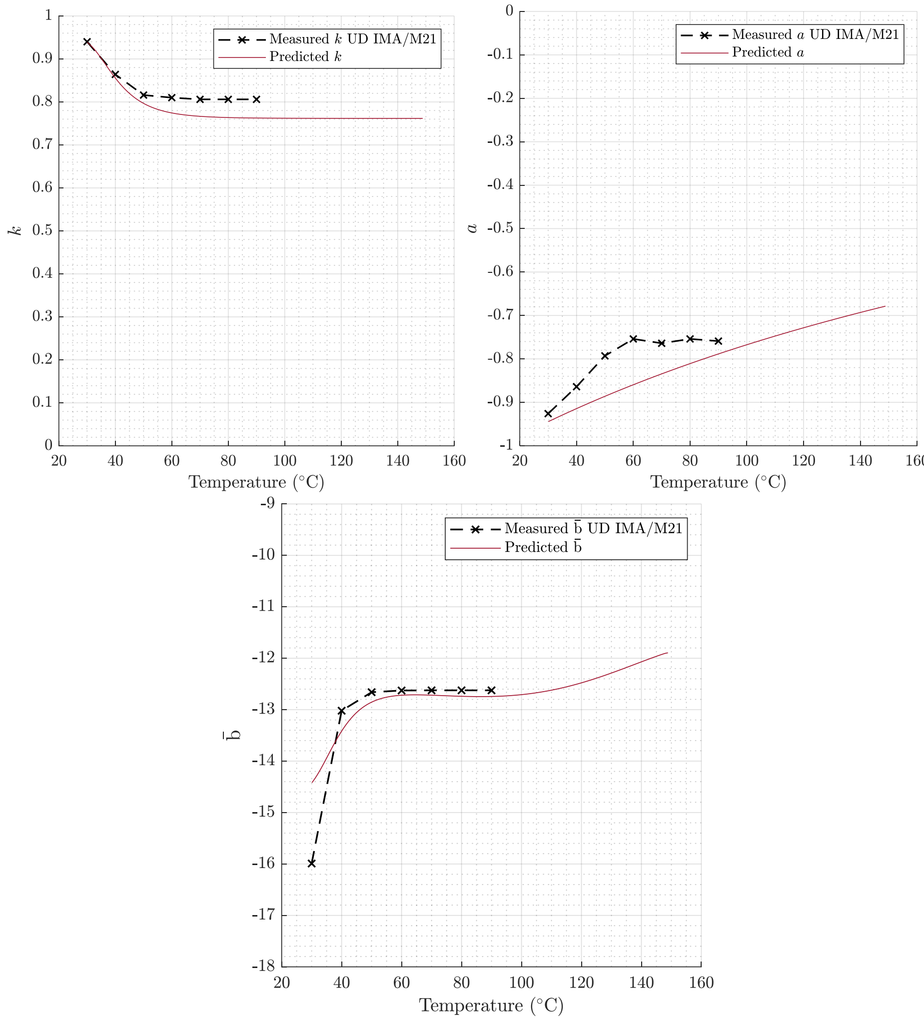

Figure 2. Model material parameters k, a, $\bar{b}$ over a range of temperatures.

3.1. Implementation of coupled cure-compaction model into ABAQUS/Standard

The previous uncoupled phenomenological model was implemented in Abaqus/Standard through a UMAT user subroutine with material parameters being linearly interpolated from experimental values taken at 10°C intervals between 30-90°C.

Due to its dependency on resin viscosity instead of experimental data, the new model was implemented for a coupled thermal-stress (cure-compaction) analysis. Consequently, an expression for the variation of stress increments with temperature was derived from the reformulated model. Heat generation caused by mechanical working of the material was assumed to be negligible. The thermal constitutive behaviour of the material, along with the evolution of resin cure and viscosity were defined in a UMATHT subroutine. An SDVINI subroutine was also added to initialise relevant variables.

3.2. Model Validation – Simulation of Cruciform Coupons

Validation of the new reformulated cure-compaction model was done using data from isothermal compaction experiments previously conducted by Nixon-Pearson et. al. [8] on 16 ply-thick cruciform coupons with a blocked ply layup.

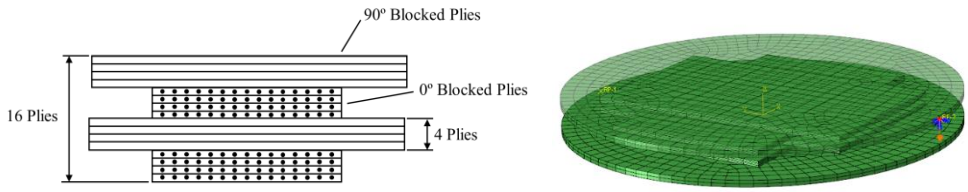

Figure 3. Layup schematic and finite element (FE) model of BP coupon.

These coupons were compacted between two heated plates and subjected to a ramp-dwell loading regime consisting of 5 equal load increments from 20 N to 60 N within 1200 s. Temperatures between 30-90°C in 10°C increments were considered. The plates were treated as rigid bodies, and the unconsolidated plies were assumed to initially be 0.22 mm thick. Experimental data was then compared to the new coupled model's predictions for final laminate thickness, in addition to the previously uncoupled model, as shown in Fig. 4.

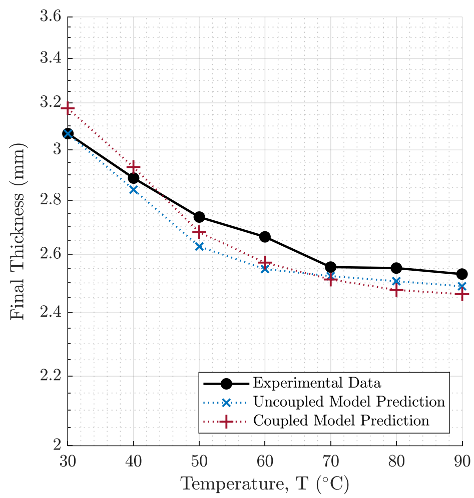

Figure 4. Final coupon thickness over a range of temperatures.

4. Coupling Coupled Cure-Compaction Model with Residual Stresses

Following from the coupled cure-compaction material model which can be used to predict the compaction of uncured toughened prepregs, focus shifted toward modelling its behaviour post-resin gelation. A material model formulated by Frerich et al. [10] was used for calculating residual stresses, which considered interleaf layers as separate to the rest of the prepreg ply and then homogenized the material according to rules of mixture derived from the force equilibrium, kinematic relations, and linear elastic constitutive equations of the thermoplastic interleafs and CFRP plies. Internal material data for IMA/M21 were used for all of the model parameters (i.e., elastic and shear moduli, Poisson's ratios, coefficients of thermal expansion (CTE), and coefficients of chemical shrinkage) of both the interleaf and prepreg layers.

4.1. Implementation of coupled residual stress-cure-compaction model into ABAQUS/Standard

The material model for predicting residual stresses was implemented as a UMAT subroutine and integrated into the coupled cure-compaction model (DefGen) via a switch function; it is assumed that prior to resin gelation, any residual stresses that may arise are free to relax and only begin to accumulate once the resin cures sufficiently. Like the coupled cure-compaction model, an expression for the variation of stress increments with temperature was also derived for the residual stress model in order to implement it into a coupled thermal-displacement analysis.

Initially, the stresses passed on to ABAQUS are calculated according to the DefGen model. As the resin's degree of cure approaches its gelation point, a hyperbolic tangent function gradually switches to passing on only the stresses calculated by the residual stress model (ResStress) as illustrated in Fig. 5, and defined in Eq. 14, where *w* is a parameter that controls the steepness of the switch.

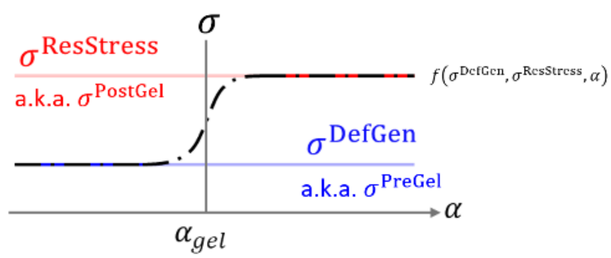

Figure 5. Visualisation of model transition upon resin gelation (for illustrative purposes of the switch function).

$$\sigma_i = f\left(\sigma^{\text{PreGel}}, \sigma^{\text{PostGel}}, \alpha\right) = \left[\frac{\left(\sigma_i^{\text{PostGel}} + \sigma_i^{\text{PreGel}}\right)}{2}\right] + \tanh\left(\frac{\alpha - \alpha_{gel}}{w}\right)\left[\frac{\left(\sigma_i^{\text{PostGel}} - \sigma_i^{\text{PreGel}}\right)}{2}\right] \tag{14}$$

In addition to this Eq. 14, derivations of switch functions for the consistent tangent operator (eq.15) and the variation of stress increments with temperature (eq.16) were also required.

$$\frac{\partial\Delta\sigma}{\partial\Delta\varepsilon} = \left[\frac{\left(\frac{\partial\Delta\sigma^{\text{PostGel}}}{\partial\Delta\varepsilon} + \frac{\partial\Delta\sigma^{\text{PreGel}}}{\partial\Delta\varepsilon}\right)}{2}\right] + \tanh\left(\frac{\alpha - \alpha_{gel}}{w}\right)\left[\frac{\left(\frac{\partial\Delta\sigma^{\text{PostGel}}}{\partial\Delta\varepsilon} - \frac{\partial\Delta\sigma^{\text{PreGel}}}{\partial\Delta\varepsilon}\right)}{2}\right] \tag{15}$$

$$\begin{aligned}\frac{\partial\Delta\sigma}{\partial\Delta T} = &\left[\frac{\left(\frac{\partial\Delta\sigma^{\text{PostGel}}}{\partial\Delta\varepsilon} + \frac{\partial\Delta\sigma^{\text{PreGel}}}{\partial\Delta\varepsilon}\right)}{2}\right] + \frac{\partial\alpha}{\partial\Delta T}\frac{\text{sech}^2\left(\frac{\alpha - \alpha_{gel}}{w}\right)}{w}\left(\frac{\Delta\sigma^{\text{PostGel}} - \Delta\sigma^{\text{PreGel}}}{2}\right) \\ &+ \tanh\left(\frac{\alpha - \alpha_{gel}}{w}\right)\left[\frac{\left(\frac{\partial\Delta\sigma^{\text{PostGel}}}{\partial\Delta\varepsilon} - \frac{\partial\Delta\sigma^{\text{PreGel}}}{\partial\Delta\varepsilon}\right)}{2}\right]\end{aligned} \tag{16}$$

4.1. Model Validation – Simulation of L-Bracket Consolidation & Detooling

Validation for the coupled residual stress-cure-compaction models was done using experimental data from Frerich [11] on 24 ply-thick L-Brackets with a [90/+45/-45/0]3s layup. For the uncoupled residual stress model, an initial ply thickness of 0.184 mm corresponding to IMA/M21's typical cured ply thickness (CPT) was used as in the original work, whereas an uncured ply thickness of 0.220 mm was used for the fully coupled simulation.

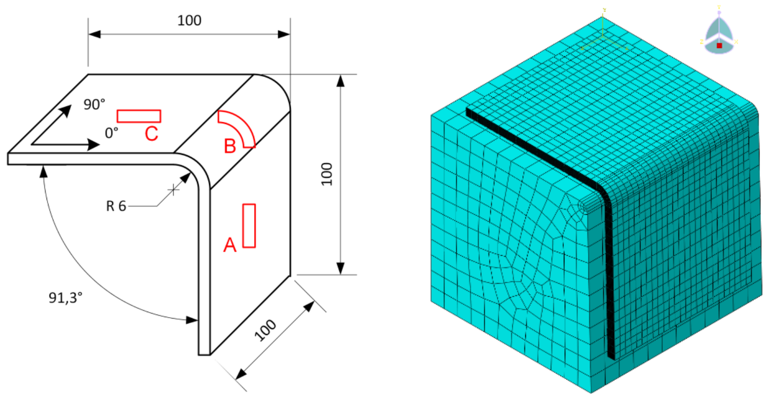

Figure 6. Schematic of L-Bracket [11] and FE model used for simulations.

The L-Brackets were compacted by a pressure force averaging around 7 bar_g and a temperature cycle consisting of two dwells at 135°C and 180°C, respectively. Detailed information on the simulated autoclave cycle is shown below in *Tables 2* and *3* [11].

Table 2. Autoclave pressure cycle used for L-Bracket simulation.

Time (s)	Pressure (bar_g)
0	0
720	6.78
15,540	6.78
15,600	6.00
27,780	6.00
28,800	0
31,200	0

Table 3. Autoclave temperature cycle used for L-Bracket simulation.

Time (s)	Temp. (°C)
0	20
4,800	135
15,600	135
18,000	180
28,800	180
31,200	20

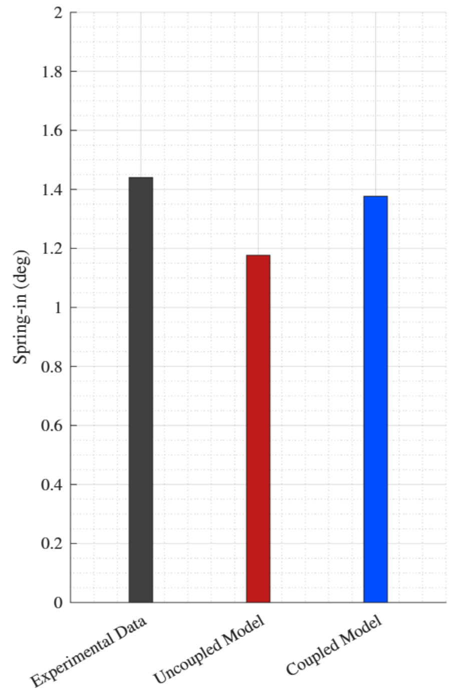

Figure 7. Global spring-in of L-Bracket; experimental and uncoupled model results from [11] compared with the new coupled model.

The global spring-in of the L-Bracket predicted using the fully coupled residual stress-cure-compaction model was compared to experimental data, as well as an uncoupled analysis using the original residual stress model [11]. The spring -in was calculated from measurements taken 20 mm and 80 mm away from one edge of the bracket, with an average predicted spring-in of 1.38°, compared to 1.44° for the experimentally observed spring-in, and 1.18° predicted by the uncoupled model (as shown in Fig. 7). The final laminate thickness was ~4.40 mm, averaging to a thickness of 0.183 mm per ply over the 24 plies, which is also in good agreement with the typical IMA/M21 CPT of ~0.184 mm [7].

5. Discussion & Conclusions

The reformulated DefGen ProToCoL model was implemented into a commercial FE package, revalidated, compared to its previous phenomenological version, and then used to simulate the autoclave consolidation of a cruciform sample. To facilitate this, models for predicting the evolution of resin cure and viscosity and other thermophysical properties relevant for heat transfer were utilised.

Predicted model material parameter values differ slightly from experimental measurements (Fig. 2), due to the new derivation of material parameters for the model reformulation considering various material systems instead of just IMA/M21. Predicted values for k and $\bar{b}$ were in good agreement with experimental measurements over a range of temperatures, with the largest discrepancy in predicted and measured values being those for a. However, a sensitivity analysis by Matveev et. al. [9] showed a is highly sensitive to other parameters which results in a high variability and has a smaller influence relative to k and $\bar{b}$. Hence, the cruciform coupons' final thicknesses predicted by the coupled model over a range of temperatures remained consistent with experimental measurements and the uncoupled model's predictions (Fig. 4).

This was further supplemented by the addition of another constitutive model for predicting residual stresses once the resin reached its gelation point. A new expression for stress variation with temperature was derived for this model in order to couple it with cure; new expressions for stress, stress variation with strain, and stress variation with temperature were also derived for the transition between the two models.

The newly reformulated coupled residual stress-cure-consolidation model is now more applicable to a wider range of material systems and process conditions, remaining capable of capturing the behaviour of prepregs and the general morphology of complex laminates following consolidation in autoclave process conditions with good accuracy. This consequently opens the door to studying the effects of non-uniform initial ply thicknesses on process-induced distortions relative to a nominal layup of uniform thickness.

6. Acknowledgements

This work was supported by the EPSRC through the Industrial Doctorate Centre in Composites Manufacture [EP/L015102/1] and sponsored by Airbus Atlantic (formerly known as Stelia Aerospace).

7. References

[1] J. P.-H. Belnoue, O. J. Nixon-Pearson, D. Ivanov, and S. R. Hallett, 'A novel hyper-viscoelastic model for consolidation of toughened prepregs under processing conditions,' Mechanics of Materials, vol. 97, pp. 118–134, Jun. 2016.

[2] J. P.-H. Belnoue, M. A. Valverde, M. Onoufriou, X. (Ric) Sun, D. S. Ivanov, and S. R. Hallett, 'On the physical relevance of power law-based equations to describe the compaction behaviour of resin infused fibrous materials', Int J Mech Sci, vol. 199, p. 106425, Jun. 2021.

[3] T. Mesogitis, J. Kratz, and A. A. Skordos, 'Heat transfer simulation of the cure of thermoplastic particle interleaf carbon fibre epoxy prepregs', J Compos Mater, vol. 53, no. 15, pp. 2053–2064, Jun. 2019.

[4] I. Hatta, T. Yamane, S. Katayama, and M. Todoki, 'The Measurements of Thermal Conductivity of Carbon Fibers', Journal of Wide Bandgap Materials, vol. 7, no. 4, pp. 294–305, Apr. 2000.

[5] G. Struzziero, M. Barbezat, and A. A. Skordos, 'Assessment of the benefits of 3D printing of advanced thermosetting composites using process simulation and numerical optimisation', Addit Manuf, vol. 63, p. 103417, Feb. 2023.

[6] L. Khoun, T. Centea, and P. Hubert, 'Characterization Methodology of Thermoset Resins for the Processing of Composite Materials — Case Study: CYCOM 890RTM Epoxy Resin', J Compos Mater, vol. 44, no. 11, pp. 1397–1415, Jun. 2010

[7] Hexcel, 'HexPly M21 Global Datasheet'. 2020.

[8] O. Nixon-Pearson, J.-H. Belnoue, D. Ivanov, K. Potter, and S. Hallett, 'An experimental investigation of the consolidation behaviour of uncured prepregs under processing conditions', J Compos Mater, vol. 51, no. 13, pp. 1911–1924, Jun. 2017.

[9] M. Y. Matveev et al., 'A numerical study of variability in the manufacturing process of thick composite parts', Compos Struct, vol. 208, pp. 23–32, Jan. 2019.

[10] T. Frerich, 'Modeling the influence of interleaf layers in composite materials on elastic properties, thermal expansion, and chemical shrinkage', J Compos Mater, vol. 53(17), Feb. 2019.

[11] T. Frerich, 'Modeling Methods for Process Induced Distortions of CFRP-Parts produced in the Prepreg-Autoclave-Process', Science-Report aus dem Faserinstitut Bremen, Jun. 2023.